

# Sedimentological and mineralogical-petrographic characteristics of Miocene evaporitic deposits (SW Erzincan)

Pelin Güngör Yeşilova\*, Şeyma Yavuz

Van Yüzüncü Yıl Üniversitesi, Mühendislik Fakültesi, Jeoloji Mühendisliği Bölümü, KAMPÜS, 65080, VAN  
[yesilovapelin@gmail.com](mailto:yesilovapelin@gmail.com), [seymayavuz639@gmail.com](mailto:seymayavuz639@gmail.com), ORCID: 0000-0002-0748-6192

## ABSTRACT

This study aimed to find the depositional environment and formation conditions of the gypsum-dominated Miocene succession alternated and intercalated with clastics and carbonates in the southwestern part of the Erzincan Basin. As a result of sedimentological, mineralogical-petrographic investigations, it was determined that the gypsum in this sequence was formed as primary and secondary. Primary lithofacies; nodular anhydrite, selenitic, discoidal, gypsum arenitic secondary lithofacies; It is divided into massive, laminated, banded, nodular, brecciated, satin-spar. The facies repetitions and folds, fractures, cracks and faulting in the sequence showed the effect of tectonism with the water level fluctuations in the basin. In addition, these investigations revealed sedimentary structures such as cross-bedding, ripple undulations, chicken-wire, enterolithic and bacterial-algal structures, parallel laminations in gypsum lithofacies. In addition to these, it was understood that gypsum lithofacies were exposed to diagenetic processes under the influence of a hot-humid and semi-arid climate, organic matter activity, meteoric/underground-water and hydrothermal solution factors, and were subjected to high temperature, pressure, salinity and pH conditions.

## ARTICLE INFO

### Research article

Received: 19.06.2021

Accepted: 16.10.2021

### Keywords:

evaporite,  
lagoon,  
playa lake,  
Miocene,  
Erzincan

\*Corresponding author

## 1 Introduction

During the Paleocene-Eocene period, the branches of the Neotethys began to close to a great extent, the existence of this ocean in Eastern Anatolia ended with the continentalization process that lasted until the end of the Middle Miocene [1]. The increase of the Cretaceous seas or the Eocene transgression enabled these seas to accumulate in the Pontide and Anatolid belts. Following this, the Eastern Anatolian Region was affected by a north-south compressional regime with the collision of Arabian-Anatolian plates in the Middle-Late Miocene [2-4]. Therefore, this combination of events led to the formation of the basins formed in this region and to contain shallow marine-terrestrial sequences reaching kilometers thick [5-7]. Erzincan basin is one of these basins and was formed in the late closure phase of the northern branch of Neo-Tethys, which separated Pontides from Anatolides during the Late Cretaceous-Early Paleocene times [8]. The basin, which became largely land after this closure, was covered by shallow seas during the Early Miocene, but these seas could not be long-lived because the region gained a overthrust structure and uplifted with north-south directional compression [8]. Intense evaporation periods

occurred in the Late Eocene-Late Miocene time interval [7, 9-11]. Tertiary evaporite deposits were formed along the line where Eskişehir-Mihalıççık, Ankara-Beyazır, Çankırı-Çorum, Sivas-Zara-Hafik, Erzincan, Refahiye-İliç, Erzurum, Tercan-Aşkale-Tekman, Iğdır-Tuzluca basins were located [12]. Volcanism products (volcanics/volcanoclastics) emerging from faults and cracks that developed due to compressional tectonism during the Middle-Late Miocene period are observed in an interbedded manner with evaporite deposits of mostly shallow-marine-terrestrial characteristics [13-16]. The study area, which is an intra-continental basin developed under the control of right lateral strike-slip fault zones and contains volcanoclastic units, is located in the southwest of the Erzincan basin and the North Anatolian Fault Zone, and in the northwest of İliç district and on the northeast edge of the Tauride-Anatoloid tectonic units [17] (Fig. 1). The gypsiferous units in the study area are distributed among Turgutlu, Küçükarmutlu, Doruksaray and Dostal Villages in the northwest of İliç district. The study area and its immediate surroundings have been studied stratigraphically, tectonically, sedimentologically, petrologically and hydrologically by some researchers [10, 18-28]. However, detailed

sedimentological, petrographic-mineralogical studies of gypsum-bearing units in the study area have not been conducted. Therefore, the purpose of this article is to contribute to regional geology by understanding the lithofacies distinctions, paleoenvironment, climate and storage conditions to be obtained by these studies.

The basis of the study area is the Upper Triassic-Upper Cretaceous allochthonous Munzur limestone, which consists of shelf type neritic limestones [19]. Later this unit is followed by ophiolites consisting of Late Cretaceous serpentinite, peridotite, gabbro and dunite. It was emplaced on the Munzur limestones with a tectonic contact. Bayhan (1982) named these ophiolites Güneş ophiolite, while Özgül et al (1981) named these ophiolites as Uluçay ophiolite. This ophiolitic unit thrusts over the flysch unit in the Middle Eocene deep sea-shelf character in the field (Fig. 1). This unit is composed of ophiolite and recrystallized limestone blocks and the alternation of limestone and clastic units (sandstone, conglomerate, siltstone) containing partly tuff and breccia levels (Fig. 1). This unit has been named as Dedek, Kozluca and Bozbel formation by some researchers [10, 19, 30-32]. Above this flysch unit is the sequence intercalated and alternated with Miocene gypsum-weighted carbonates and clastics, which are the subject of our study, with an angular unconformity (Fig. 1). These evaporites are mostly primary and secondary gypsum and contain anhydrite in places. The clastics found together with the evaporites are predominantly sandstone, mudstone and claystone, while carbonates are limestone and dolomite [10, 33-35]. These units are laterally and vertically transitive with each other. Kurtman (1973) distinguished the lower parts of this sequence as Karacaören Formation and the upper parts as Hafik Formation. According to the fossils in the clastics belonging to these two formations, the age of the evaporitic sequence extends from Lower Miocene to Upper Miocene [32]. However, since there is no unconformity between the two formations and they have

lateral and vertical transitions, this article has been investigated as a whole under the name of Miocene evaporites. This gypsiferous unit is bedded, faulted, fractured and occasionally folded. These folds originated from the Alpine orogeny that occurred at the end of the Miocene [10]. All these units are respectively covered by Pleistocene terrestrial clastics (conglomerate, sandstone, claystone and siltstone) and Quaternary alluviums [19] (Fig. 1). This Miocene sequence is sometimes observed as overthrust by the Upper Cretaceous ophiolitic melange in the study area [19, 35-36].

## 2. Methodology

This study consists of research, field and laboratory studies. During the field study, measured stratigraphic sections were prepared for the areas where Miocene evaporites were observed well, and systematic sampling was performed for mineralogical-petrographic analysis. Accordingly, 30 of the samples collected from the field were prepared for thin section and made in Dokuz Eylül University Thin Section Laboratory. Since the water of crystallization disappears when samples containing gypsum is heated and bassanite is formed, the grinding of the samples was done using machine oil instead of water. Then, the epoxy used in thin section production was hardened at room temperature and this harden process was continued by heating in the drying oven. After the adhesion process was completed, thinning was made with abrasives varying between 400 and 800 microns and the photos of the sections presenting features were taken with a Leica model microscope. In addition, the Scanning Electron Microscope (SEM-EDS) analysis on 10 gypsum samples was carried out at the Scientific Research and Application Center of Van Yüzüncü Yıl University. The gypsum samples were coated with Au-Pd and examined by scanning the sample surface with an electron beam in the ZEISS Sigma 300 model SEM microscope and photographed with the SE2 detector.

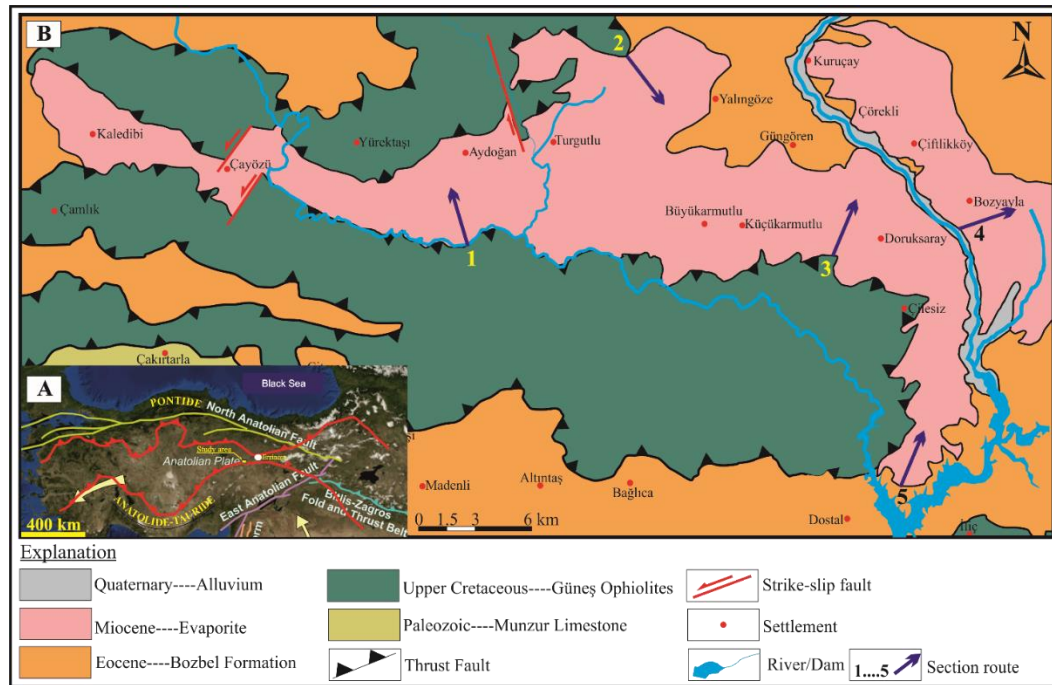


**Figure 1.** (A) Location of the study area. (B) Geological map of the study area (1/25000).

### 3. Results and discussion

#### 3.1. Sedimentology

Existing sedimentological studies have been carried out on Miocene evaporitic units around Doruksaray and Dostal villages. These evaporitic units are mainly consist of primary (selenitic, gypsum arenite and discoidal gypsum rosette) and secondary gypsum lithofacies (such as masive, masive-bedded, massive laminated, nodular, nodular-banded, laminated and laminated-banded and satin-spar) with nodular anhydrite. In the study area, 5 measured stratigraphic sections were taken from the localities where evaporitic lithofacies are best observed, and as a result of their correlation, a general evaporitic sequence with a thickness of approximately 300 m was obtained (Fig. 2). Primary and secondary gypsoms in this sequence are alternated with each other at some levels, and at some levels are intercalated, inerbanded and alternated with volcanoclastic (tuff and volcanic gravel), basalts, red, green

and gray clastics (gravel, sand, clay and mudstone) and carbonated units (limestone and dolomite) (Fig. 2). Secondary gypsum derives mainly from hydration of primary anhydrite rocks or from dehydration-rehydration processes of primary gypsum. These secondary gypsum generally show alabastrine and porphyroblastic textures in the field. Alabastrine texture is milky white, homogeneous and fine-grained, while porphyroblastic-textured gypsum is more medium-coarse-grained and the grains are observed to float in alabastrine gypsum texture. These textures are easily distinguished with the naked eye in the field and sometimes appear together. Some sedimentary structures (such as enterolithic, undulated, folded, bedded, brecciated, cross-bedded, parallel laminated) are observed in all these gypsum-bearing sequence with the effect of regional tectonics, climate and strong diagenesis. In addition, there are faults, deformations and inter-banded of ferrous-mangane alterations in some areas.

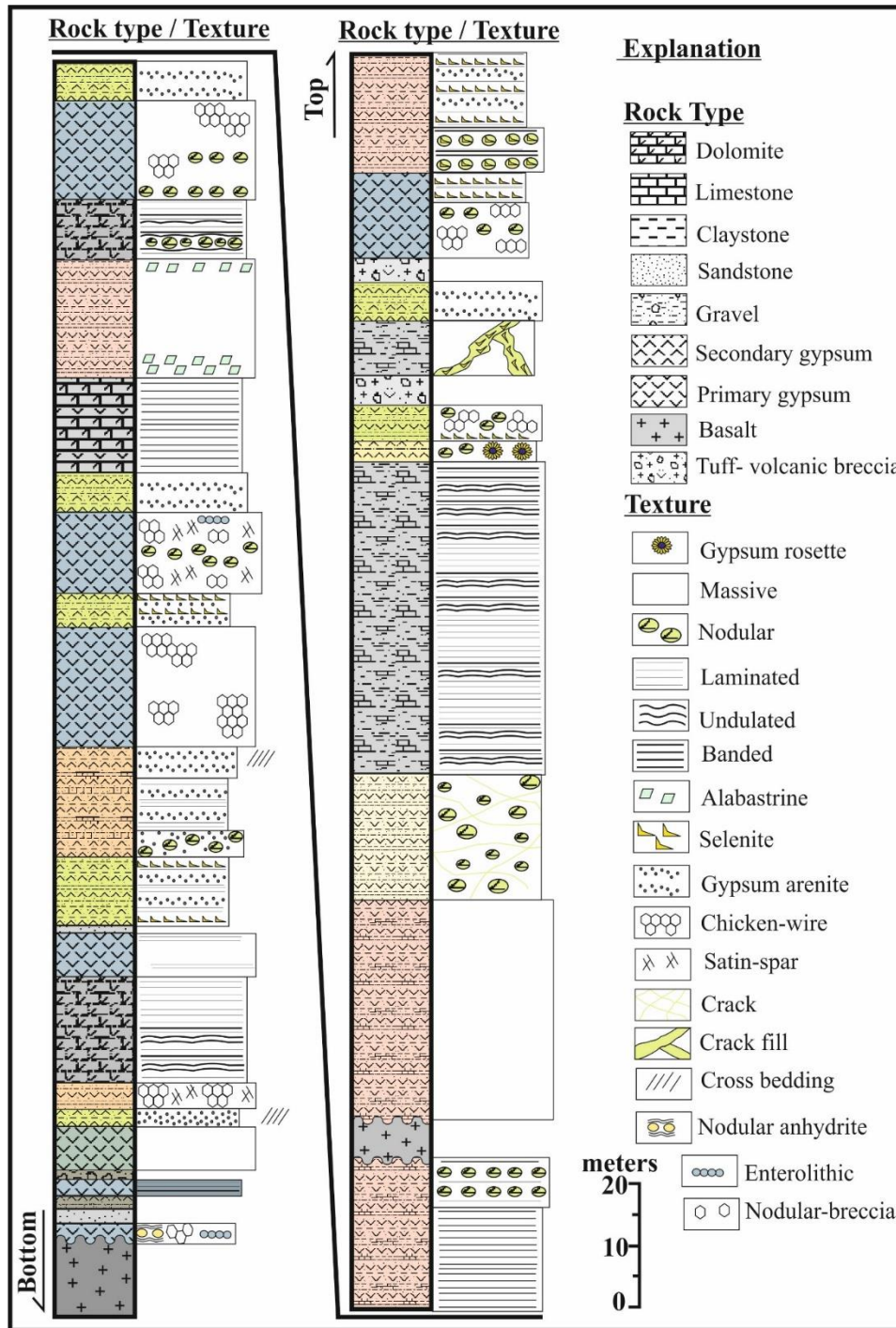


**Figure 2.** Generalized measured stratigraphic section of the Miocene evaporites.

The anhydrite nodules observed in the field were formed by the combination and growth of primary anhydrite lats in the unconsolidated red-brownish carbonated mud in the syn-sedimentary stage [37]. Carbonated mudstone is accumulated in subaqueous conditions during dilution of brine in an evaporite environment. These are then partially or completely transformed into secondary alabastrine and porphyroblastic gypsum at the end of early and/or late diagenetic processes.

Nodular anhydrite is mostly formed in sabkha environment dominated by terrestrial conditions [38]. These anhydrites are separated from each other by a light brownish and carbonated mud matrix in the study area. They consist of a mosaic of white nodules and their diameters vary between 0.1-10 cm (Fig. 3A). These nodules exhibit some levels of chicken-wire internal structure. The splicing of nodular anhydrites with each other in the sabkha environment are formed the chicken-

wire cage structure [39] (Fig. 3B, C). Due to the continuous sedimentation, tectonic deformation, volume changes in rocks and excessive pressure, the nodules acquire a ductile fluid property and acquire a folded enterolithic-like structure in the study area [40].

The free-grown-twinning selenitic gypsum are observed in different crystal types, colors and sizes in the study area. Crystal shapes and sizes of selenitic gypsum give information about the temperature, acidity and organic matter content of the environment. In addition, environmental salinity change rates and refreshing periods can also cause different types of selenite crystallization [41]. These gypsum are fine to medium coarse crystalline (1 micron-40 cm) and transparent, and cleavage and twinning levels can be distinguished by the naked eye (Fig. 3D, E). Selenitic gypsum precipitates directly from brine and grows freely upward from the sediment-brine interface (Fig. 3E). They are sometimes observed in the study area in the form of freely grown in gray colored or red carbonate-clayey mudstones or with clay-carbonate interband and sometimes as a crack fill in mudstone (Fig. 3E, F). Selenitic gypsum crystalline mudstones reflect dry-shallow lake environment conditions [42-43]. Fine to medium grained selenitic gypsum are sometimes cemented together with carbonate and gypsum matrix (Fig. 3G, H). The presence of longitudinally developed and clustered prismatic selenites (Fig. 3I) in the study area indicates that acidic conditions prevail in the sedimentation environment, while the presence of lenticular, dark brown-black colored selenite crystals (Fig. 3G, I, J) can be attributed to the organic matter [44]. The rosette-shaped crystal cluster of selenites (Fig. 3K) is formed by the combination of very high organic matter content and temperature factor in the environment [45]. Ground-water is effective for this type of gypsum, which reflects the lake-shore swamp environment [46-47]. Selenitic gypsum is sometimes bedded, laminated, folded and undulated, while those with medium grains are alternated with gypsum arenites (Fig. 3L). In addition, microfaults, anhydritization and carbonation

bands are occasionally encountered among these (Fig. 3M). The gypsum arenite lithofacies, which is the size of clastic sand, which is formed by the separation of selenitic gypsum lithofacies by the effect of waves and re-working and deposition, is another a lithofacies in the study area (Fig. 3B). Among these, cross-bedding, ripple corrugations, laminations, and clastic and carbonate intercalations are common (Fig. 3L, M, N). This type of gypsum is mostly settled in the shallow water-shore side of the salt water body [48-49]. The primary discoidal gypsum rosettes observed in the sequence were developed by displacement in organic matter rich claystone and red colored mudstone [37-38, 50-51] (Fig. 3K). Later, these primary gypsum are diagenetically transformed into anhydrite and secondary gypsum, respectively (Fig. 3J). The observation of gypsum arenites together with the nodules in the sequence proves that some of these secondary gypsum originate from the primary gypsum origin (Fig. 3B). Separate concentric salt solutions are formed as a result of the addition of evaporitic ground-water into the cracks and a mud-flat rich in organic matter (humic acid) that rises to the surface during the drying phase of the environment. High concentrations of sulfate and calcium in ground-water lead to the replacement of these salt solutions in-situ and then crystallization of these solutions into a as discoidal gypsum rosettes [51, 54-55]. Humic acid is a type of acid produced by bacteria under reducing environment conditions. The fact that the crystal sizes in discoidal gypsum are approximately equal to each other (approximately 0.2-0.5 cm) shows that the salinity and temperature conditions at these levels of the sequence are not very variable (Fig. 3K). There are areas rich in red colored Fe-oxide in these parts. Selenitic gypsum in most levels of the sequence are alternated and intercalated with secondary gypsum (Fig. 3O). This alternation; It is important in terms of showing that gypsarenites transform into anhydrite with the effect of the salinity of the evaporating brine and then re-form secondary gypsum through rehydration.

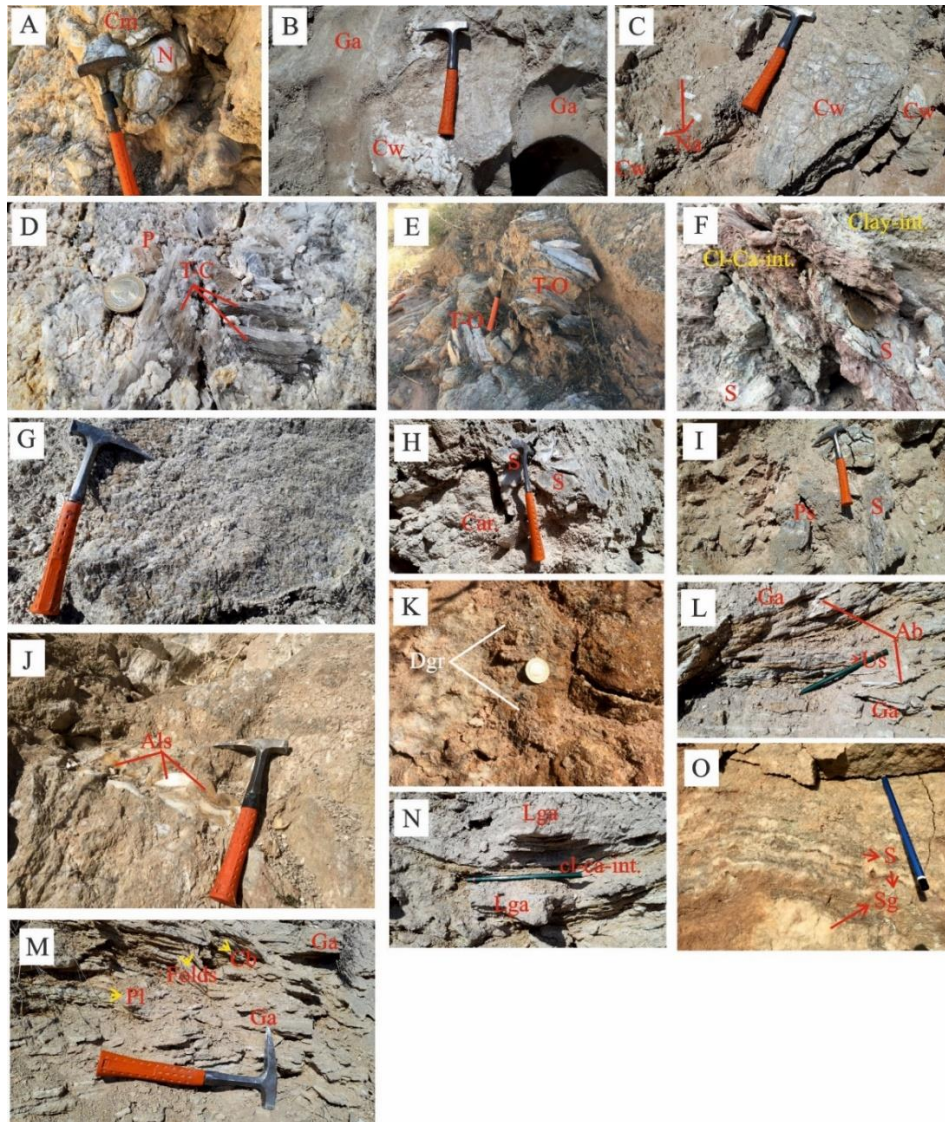


**Figure 3.** Sedimentologic aspects of gypsum lithofacies. (A) Anhydrite nodules (N) within the carbonated mudstone (Cm). (B) Nodules showing chicken-wire interior structure in gypsum arenites (Ga). (C) Anhydrite nodules (Na) and chicken-wire structures (Cw) in selenites. (D) Twinned-cleavage (T-C) selenites and prismatic (P) selenites rich in organic matter. (E) Carbonated, coarse crystallized, organic matter containing (O) dark colored and twinned (T) selenites. (F) Selenite (S) with clay carbonate intercalations (Cl-Ca-int). (G) Fine to medium grained selenitic gypsum cemented together with a gypsum matrix. (H) Medium grained, prismatic selenitic gypsum (S) cemented together with a carbonate (Car) matrix. (I) Longitudinally developed and clustered (S) prismatic selenites (Ps). (J) Anhydritized (A), brownish and lenticular (l) selenite (s) level. (K) Discoidal gypsum rosettes (Dgr) within the red mudstone. (L) Undulated selenites (Us) alternated with gypsum arenites (Ga) and alabastrine gypsum (Ab). (M) Cross-bedded (Cb) and folded gypsum arenites (Ga). (N) Laminated gypsum arenite (Lga) with clay-carbonate intercalations (cl-ca-int). (O) Undulated selenite (S) gypsum alternated with secondary gypsum (Sg) levels and nodules.

Massive gypsum shows a rhythmic alternation with red mudstones and are sometimes observed as laminated and banded and sometimes bedded (Fig.4A, B).. The presence of lamina and bands in massive gypsum is important in terms of showing shallow water environments [37, 56]. Massive gypsum varied in thicknesses between 3-25 m in the sequence and transformed into white colored homogeneous alabastrine or porphyroblastic texture secondary gypsum in the late diagenetic phase (Fig. 4C). Mudstones are characterized by

massive textured red claystone and siltstone (Fig. 4D). The alternation of these gypsum with red mudstones is probably evidence that the climate changes periodically to arid and semi-arid [9, 57]. This alternation shows that terrestrial sedimentation has developed and evaporation is interrupted from time to time due to the gradual decline of the sea [58]. However, in some outcrops these gypsiferous red mudstones transition to gray-green claystones. This transition is an indication that the playa lake can reach the sea [9, 59].

However, the fact that the massive gypsum is interlayered with grayish-green sandstones with a thickness of approximately 1 m at some levels in the sequence and cream-beige colored marl and limestone indicates that the depositional conditions are sometimes subaqueous and deeper conditions [9, 60] (Fig. 4E). Massive layers show a chicken-wire texture with undulated and tepee structure type folds at most levels of the sequence (Fig. 4F). These structures are formed as a result of the effects of climate and diagenesis and show that these gypsum sometimes came out subaerial of water [39, 47, 55, 61]. In addition, the presence of chicken-wire texture in this gypsum and the alternation of these gypsum with red clastics indicates the transition from sea conditions (by fresh water inputs) to very shallow and highly salty environments separated by a barrier [9, 59]. Laminated, laminated-banded gypsiferous lithofacies contain clay-carbonate inter-bands and intercalations and some levels alternate with carbonates in the field (Fig. 4G, H). These structures are indicative of a shallow water environment such as a lagoon [62-63]. Laminas contain nodules of white gypsum that range in size from 5 to 20 cm (Fig. 4I). The reason of this; It is the decrease of the water level in a shallow water environment such as a lagoon, followed by the introduction of sulfate-rich groundwater and a partial dissolution in laminated gypsum and the salinity of the brine water increases as a result of evaporation. Hence, nodular gypsum precipitates instead of laminated gypsum [64]. Lamina thickness is 1 cm or less, and band thickness varies between 1 cm and 10 cm. There are undulations, parallel laminations, fractures and folds in these structures and these structures (Fig. 4I) reflect high energy shallow water conditions [65]. The nodular, nodular-banded, nodular-laminated and nodular-breccia gypsum lithofacies are usually found in sandy carbonate and mudstone. White

nodules with a diameter of approximately 0.5 to 5 cm come together and exhibit a nodular banded or laminated appearance (Fig. 4J, K). These lithofacies are sometimes in the form of irregular nodules in the field, partially or completely separated from each other by mudstone and / or carbonate matrix. These are often observed within the massive and laminated gypsum layers, sometimes between gypsum arenite and selenite layers, and may show chicken-wire and enterolithic internal structures (Fig. 3O, 4L). The observation of these structures indicates that the temperature, pressure and salinity conditions are increasing. Nodular gypsum, which displaces within the carbonates, are both derived from the hydration of nodular anhydrites, and also derived from the anhydritization of selenitic gypsum in the early-late diagenetic phase and rehydration in the late diagenetic phase (Fig. 4L). These gypsum exhibit secondary alabastrine and porphyroblastic textures. Breccia-nodular gypsum lithofacies, on the other hand, is an eroded gypsum formed as a result of intense tectonism simultaneously with sedimentation, which became active in the last stage of evaporite deposition in the studied basin (Fig. 4M). All these nodular lithofacies denote sabkha or mud-flat environments [38, 50, 66]. Since tectonic activities affected the basin, brecciation occurred throughout the deposition. As a result of dissolution in carbonates and nodular and laminated gypsum, veins and fractures varying between 0.5 and 2 cm in thickness and mudstone cracks were filled with satin-spar gypsum. Satin-spar gypsum crystals are oriented and their long axes are perpendicular or semi-parallel to the vein walls and their widths vary between a few mm and cm (Fig. 4N). These gypsum are formed in mud flat-sabkha environments [38, 67].

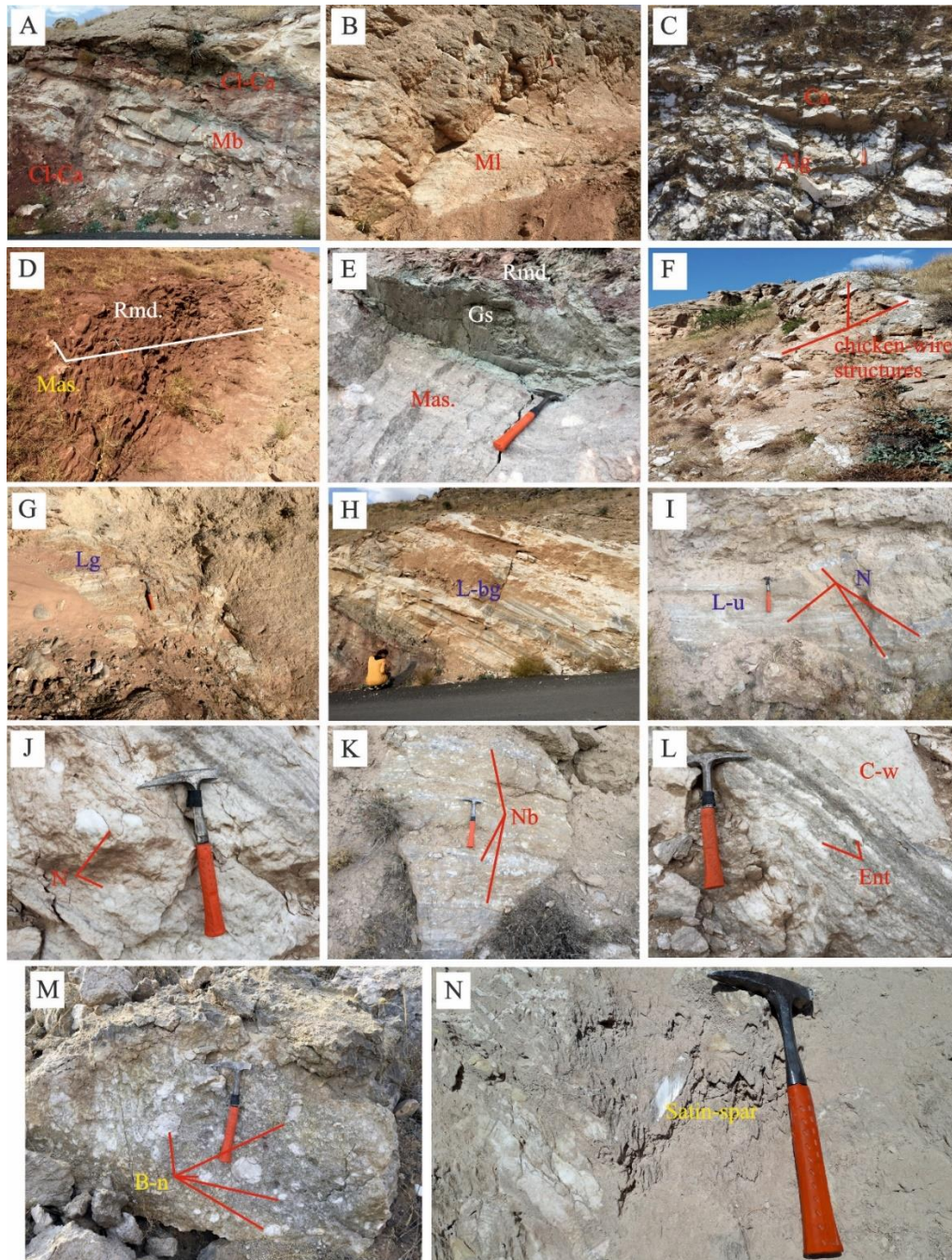


**Figure 4.** Sedimentological aspects of secondary gypsum lithofacies. (A) Massive-bedded (Mb) gypsums alternated with clayey (Cl) and carbonated (Ca) units. (B) Massive-laminated gypsums (Ml). (C) Massive alabastrine secondary gypsum (Alg) alternated with carbonates (Ca). (D) Massive gypsums (Mas) within the red mudstones (Rmd). (E) The alternation of red mudstones (Rmd) and green sandstone (Gs) between massive (mas) gypsum levels. (F) Chicken-wire structures in the massive gypsums. (G) Laminated gypsums (Lg). (H) Laminated-banded gypsums (L-bg). (I) Nodular (N) structures within the laminated-undulated (L-u) gypsums. (J) Nodular (N) alabastrine secondary gypsum. (K) Nodular-banded (Nb) gypsums. (L) Chicken-wire (C-w) and enterolithic structures (Ent) in the nodular gypsum levels. (M) Brecciated-nodular (B-n) gypsums within the clayey carbonates. (N) Satin-spar gypsums within the grey mudstone cracks.

#### a. Petrography

It is determined most secondary gypsum textures were alabastrine, porphyroblastic, sutured-bounded

porphyroblastic, mosaic, microcrystalline, nodular, mosaic, nodular banded, brecciated and satin-spar textures with primary selenitic and arenitic gypsums in petrographic studies. Secondary gypsum textures are formed either directly from anhydrite or by dehydration (losing the water in its body)

of primary gypsum and then rehydration. Hydration channels are clearly observed in porphyroblastic gypsum. The greatest evidence of these events is the presence of anhydrite relicts in the form of euhedral, very coarse crystalline and sometimes euhedral prismatic crystals in porphyroblastic gypsum (especially in nodular gypsum) (Fig. 5A). The anhydrite relicts show 3rd order vibrant interference colors, their sizes are between 0.1 mm and 0.4 mm, the optical relief is medium (Fig. 5A). In addition, the presence of pseudomorphic secondary gypsum that preserves the crystal structure of tabular primary gypsum proves that some of these secondary are derived from primary gypsum (Fig. 5B). These two textures, which show the effect of dissolution and recrystallization processes in some sections, are observed in each other. Generally, alabastrine texture is formed by recrystallization of porphyroblastic textured gypsum. Porphyroblastic gypsum is medium-coarse grained (1-2 mm), with marked grain boundaries, showing first order interference colors, and cleavage marks have not disappeared yet, although they are in the advanced stage of diagenesis (Fig. 5C). Alabastrine texture is dominated by a lacy texture with lost grain boundaries and interlocking and inter-twined optical properties (Fig. 5D). If this texture consists of very fine grained gypsum crystals (approximately  $1\mu\text{m}$ ), it is called microcrystalline massive texture (Fig. 5E). This texture is formed by dissolution and recrystallization of gypsum crystals by the brine coming in the flooding period [68]. Chicken-wire texture is observed in thin section studies of these massive gypsum samples (Fig. 5F). Alabastrine texture development occurs under conditions where contact with water is excessive, and is observed in thin sections as replacing porphyroblastic gypsum [68] (Fig. 5C). Simple twinning is

observed in both gypsum textures. Late diagenetic euhedral, semi-euhedral and anhedral calcite minerals in all secondary textures are observed in thin sections, replacing secondary gypsum with the effect of carbonate-rich surface waters (Fig. 5G). At the same time, black colored organic matter relicts and carbonation areas replacing with grains around the grains are observed in some of these types of porphyroblastic gypsum (Fig. 5H). The observation of sutured-bounded porphyroblastic secondary gypsum (Fig. 5A) in some thin sections indicates that they were formed before alabastrine gypsum [69]. Along with these, nodular gypsum framed with micritic mud and interlocking chicken-wire texture are frequently observed. The nodular-brecciated banded structures formed by the combination of brecciated or nodular gypsum are clearly observed (Fig. 5I). In addition, satin-spar gypsum perpendicular to the vein wall filling the cracks of secondary alabastrine porphyroblastic textured gypsum or micritic textured limestones are also encountered (Fig. 5J). These cracks were formed due to the increase in volume during conversion from gypsum to anhydrite or from anhydrite to gypsum.

In optical microscopic examinations, selenitic gypsums are fine-medium-grained, euhedral-subhedral prismatic, tabular forms, first order colors, unidirectional cleavage and twinning (Fig. 5K). These gypsum transformed into alabastrine and porphyroblastic textured gypsum in the advanced stages of diagenesis. The arenitic gypsum texture is composed of sand-sized gypsum formed by selenite recrystallization [70] (Fig. 5L). The spaces between the grains are filled with carbonate, clay cement and detritic material.

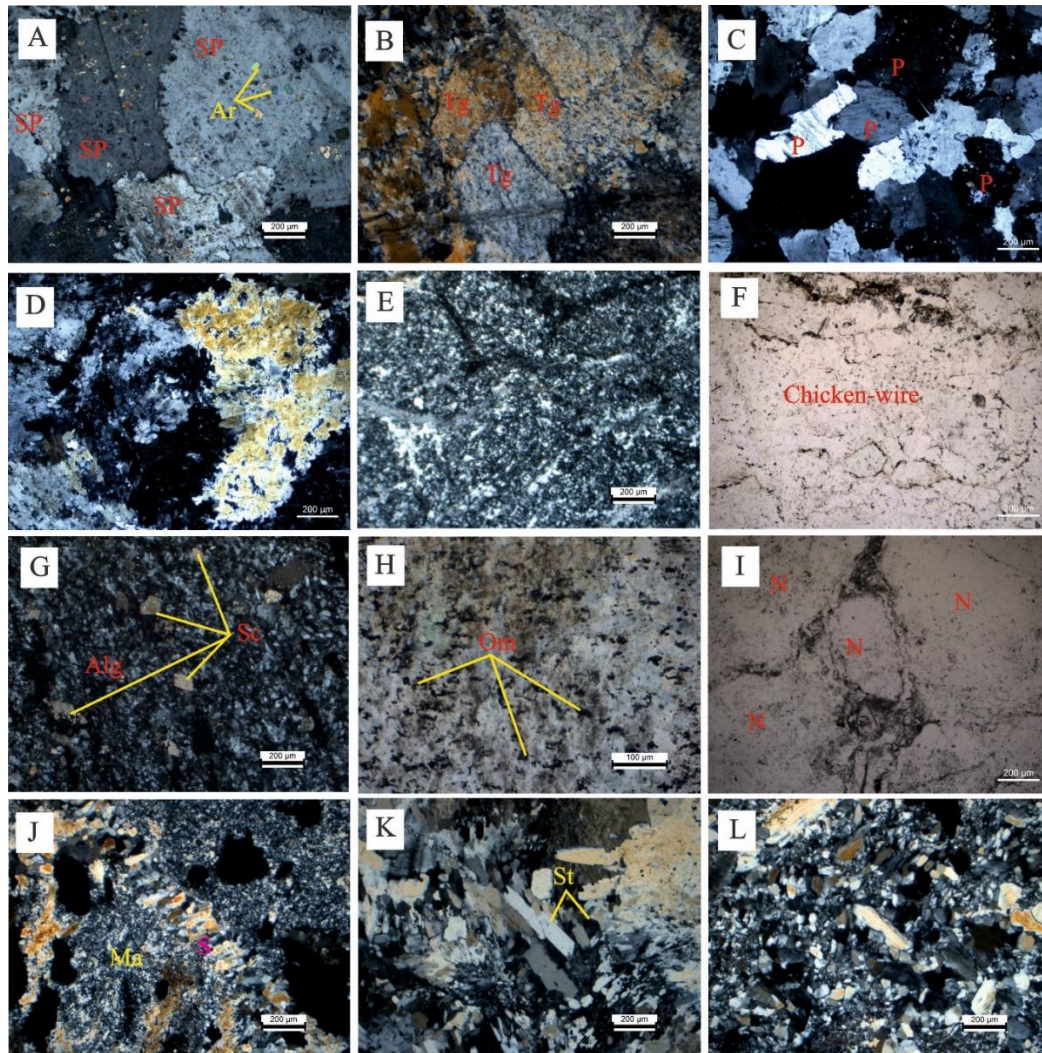


**Figure 5.** Petrographic aspects of gypsum lithofacies. (A) Sutured-bound porphyroblastic (SP) gypsum with anhydrite relicts (Ar) in them. (B) Pseudomorphic secondary gypsum formed as a result of dehydration-rehydration processes of tabular gypsum (Tg). (C) Porphyroblastic (P) gypsum with clear grain boundaries preserving cleavage marks. (D) Alabastrine textured secondary gypsums. (E) Microcrystalline tectured alabastrine gypsums. (F) Chicken-wire structures. (G) Euhedral and semi-euhedral secondary calcite (Sc) crystals replaced by alabastrine secondary gypsum (Alg). (H) Organic material (Om) relicts within the secondary gypsums. (I) Nodular (N)-brecciated structures. (J) Satin-spar (S) gypsums within the microalabastrine (Ma) secondary gypsum texture. (K) Simple twinned (St) selenites. (L) Arenitic gypsum texture.

#### b. Mineralogy (Sem)

In order to determine properties such as micro-textural, crystal morphologies and relationships with other minerals in gypsum samples belonging to the study area, image examinations performed with Scanning Electron Microscopy (SEM) and

quantitative analysis were performed by EDS studies. As a result of SEM studies, gypsum ( $\text{CaSO}_4 \cdot 2\text{H}_2\text{O}$ ), orthorhombic celestine ( $\text{SrSO}_4$ ) and dolomite (Ca-Mg carbonate), calcite ( $\text{CaCO}_3$ ) and some iron-rich minerals, clay and siliciclastic minerals (such as quartz, feldspar) were observed.

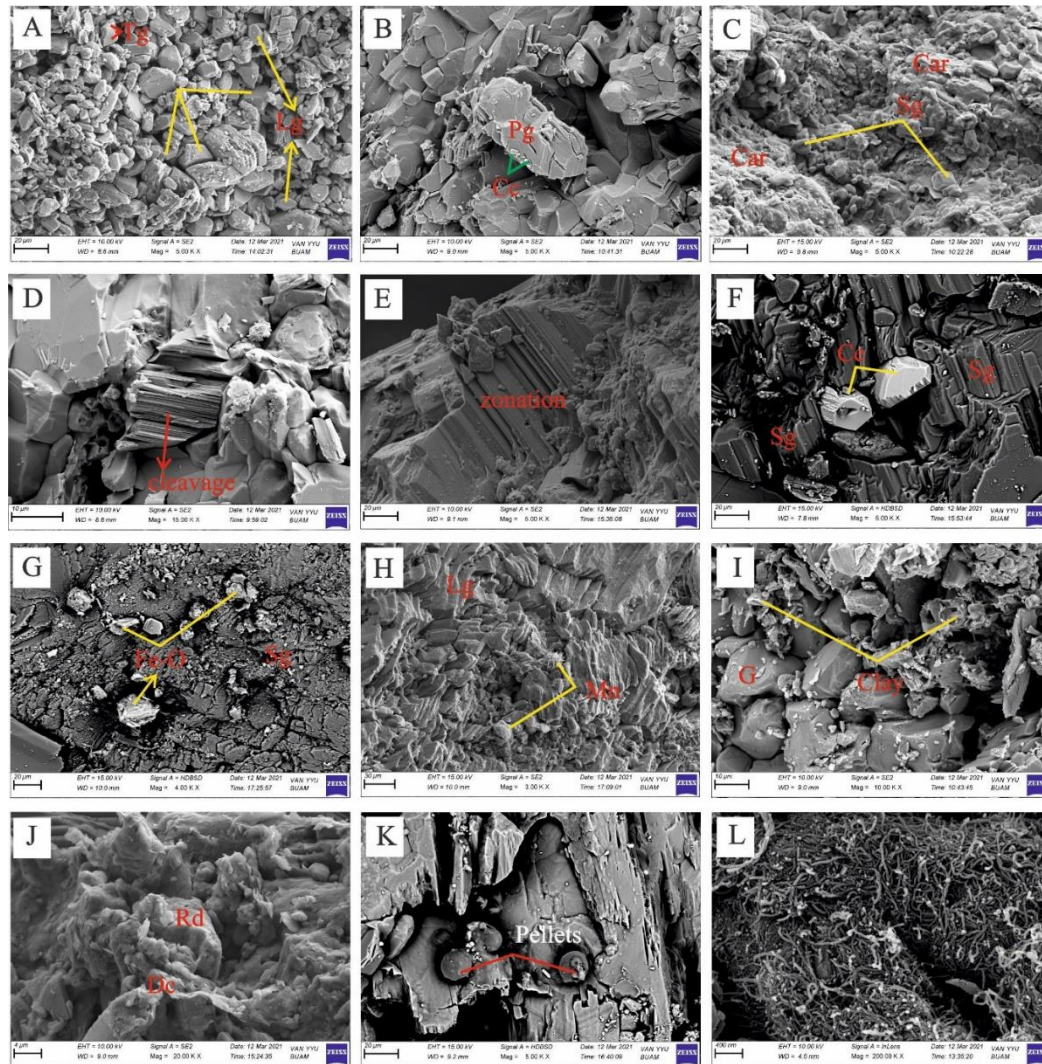


**Figure 6.** SEM images of gypsum lithofacies. (A) Tabular (Tg) and lensoidal (Lg) primary gypsums. (B) Folds and ruptures in prismatic gypsum (Pg) with calcite cement (Cc). (C) Late diagenetic carbonation (Car) in secondary gypsum (Sg). (D) Cleavage in prismatic gypsum. (E) Zonation of gypsum. (F) Celestine minerals replaced with secondary gypsums. (G) Minerals rich in Fe-oxide in secondary gypsums. (H) Manganese (Mn) formations in laminated gypsum (Lg). (I) Plate-like clay formations with gypsum (G). (J) Detritic clay minerals secondary replaced with rhombohedral dolomite minerals. (K) Pellets in the gypsums. (L) Bacterial-algal structures.

During the early diagenesis, dolomite mineral was observed, which replaced calcite. The Mg-rich liquids caused the formation of dolomite instead of calcite with surface alteration. Gypsum are generally prismatic, tabular and lenticular and contain fractures and folds due to deformations (Fig. 6A, B). The presence of these smooth surfaces in gypsum can be attributed to the high temperature, salinity and pH conditions [42]. In the late diagenetic phase, carbonation with the effect of carbonate-rich surface waters and also detrital clay minerals carried into the gypsum are common in gypsum (Fig. 6C). Cleavage marks are evident and there are calcite cements along the cleavage surfaces (Fig. 6D). Selenitic crystals follow each other in the form of transparent and zoned growth structures and are in the form of dark-light colored zones (Fig. 6E). There are carbonate inclusions along the growth surfaces. Inside the prismatic gypsum, the mineral of

the celestine replacing the white gypsum was found (Fig. 6F). Diagenetic solutions rich in strontium (waters released during gypsum anhydrite transformation) or hydrothermal related waters mix with groundwater, allowing the reaction of Sr and Ca in the late diagenetic stage. Thus, the mineral of celestine rich in  $\text{SrSO}_4$  is formed instead of gypsum [71-72]. At the same time, high amounts of iron-rich hematite or magnetite type Fe oxide minerals, very high amounts of manganese and Fe-rich Ca, Mg, Al silicate minerals (smectite, saponite type) were detected in these gypsum (Fig. 6G, H, I). These minerals are observed in a fine-grained plate-like form and have a grain size of  $\leq 10\mu\text{m}$  (Fig. 6I). The presence of these clay minerals is important in terms of showing that the climate is humid-hot and dry and shallow water conditions [37, 73-74].

Apart from these, some metallic elements (Co, Cu, Ni, Zn, Zr) were detected in the EDS study. All these elements, including Mn and Fe elements, were probably transported into gypsum by hydrothermal solutions passing through the fractures and faults in the basin and created hydrothermal alteration zones observed in the study area [75]. High observation of Rb element in some samples in EDS study indicates that dolomite content increased in these gypsum samples [76] (Fig. 6J). These dolomites were replaced by detritic clay minerals in the late diagenetic phase (Fig. 6J). In some gypsum samples, pellets with a grain size of 10µm in general, equal size and with a smooth surface and spherical morphology were detected (Fig. 6K). Pellets are formed in environments with high organic material and bacteria content [77]. These are carbonate grains formed in subtropical environments [78]. In addition to these, bacterial-algal structures have been found (Fig. 6L). These structures generally show shallow water conditions and the region close to the coastline [79-80]. Laminated gypsum was found on SEM images, and lamination thicknesses vary between 1 and 2 µm. It has been observed that the lamination surfaces are quite smooth, but sometimes there are indentations and protrusions (Fig. 6H).

#### 4. Conclusions

Lithofacies and sedimentary structures distinguished in the study area were decisive in terms of the deposition environment and formation conditions. Accordingly, while primary lithofacies such as gypsarenite and selenite were deposited at the margins of the basin (such as coastline-sabkha), discoidal gypsum rosettes and satin-spar gypsum were deposited in intra-continental areas such as mud flats-sabkha or playa, where regressed of saline waters related to ground-fresh water intake. In addition, cross-bedding, ripple undulations, green clay interlayers (smectite, saponite) and red clast alternates within these showed a playa lake environment formed by temporary streams developed under arid-semi-arid and hot-humid climatic conditions. The laminated and banded lithofacies and parallel laminations, folds and bacterial-algal structures observed within the units mostly marked shallow sea-lagoon environments, while all of the chicken-wire, enterolithic and nodular lithofacies were deposited on the sabkha and salty mud flats. Massive gypsum deposited relatively deeper parts of the basin due to the uplift of the basin. Therefore, due to climatic-seasonal changes and tectonic effects, it is observed that the basin where gypsum-dominated lithofacies deposited deepened over time, then became shallow and gradually dried up completely. It is understood that facies change depending on these different conditions. According to all these facies changes, sedimentary structures, and the alternation and transition of these lithofacies with red and green clastic units and carbonate units, the basin is of a size reaching up to the lagoon-coastal sabkha-playa lake which separated by a barrier from the shallow sea [37, 81]. In addition, it was determined that they were subjected to some diagenetic processes (volumetric shrinkage,

recrystallization, dissolution and replacement, etc.) under the varying temperature, pressure, salinity and pH conditions, and as a result, they exhibit mineralogical, structural and textural changes as a result of sedimentological petrographic and mineralogical investigations of the evaporitic units.

The presence of dark colored (brown-black) and smaller gypsum crystals and pelloidal structures determined by sedimentological and mineralogical studies showed that organic / bacterial activity was intense and environmental conditions were more reducing and acidic. The high amounts of metallic elements (such as Fe, Zn, Ni, Co) in gypsum detected in the SEM-EDS study can be attributed to the fact that they may have been transported from the bedrock by washing with hydrothermal solutions in the post-deposition. In addition, the presence of volcanoclastic levels and celestine mineral in the gypsum in the sequence showed the effect of possible active hydrothermal solutions rising from the faults limiting the basin, depending on the activity of the volcanism and tectonic activity during the Middle-Late Miocene in the region. These solutions were formed intermediate bands with hydrothermal alteration, rich in iron-manganese determined in the SEM studies, between the evaporites.

#### Acknowledgements

This study was carried out within the scope of Yüzüncü Yıl University Scientific Research Projects project no " FYL-2019-8742". I would like to thank Çetin Yeşilova for their contribution in the preparation of the article and field studies.

#### References

- [1]. Brinkmann, R., "Geology of Turkey", Elsevier, Amsterdam, (1976), 158.
- [2]. Açlan, M., Altun, Y., "Syn-collisional I-type Esenköy Pluton (Eastern Anatolia-Turkey): an indication for collision between Arabian and Eurasian plates", J. African Ear. Sci., 142, (2018), 1–11.
- [3]. Oyan, V., "Ar-Ar dating and petrogenesis of the Early Miocene Taşkapı-Mecitli (Erciş-Van) granitoid, Eastern Anatolia Collisional Zone, Turkey", Journal of Asian Earth Sciences, 158, (2018), 210-226.
- [4]. Şengör, A. M. C., Yılmaz, Y., "Tethyan evolution of Turkey: a plate tectonic approach" Tectonophysics, 75, (1981), 181–241.
- [5]. Hall, R., "Ophiolite emplacement and the evolution of the Taurus Suture Zone, southeastern Turkey", Bull. Geol. Soc. Am., 87, (1976), 1078-1088.

- [6]. Kurtman, F., Akkuş, M. F., Gedik, A., "The geology and oil potential of the Muş-Van region", *Miner. Res. Explor. Inst.*, 169, (1978), 124-133.
- [7]. Koşun, E., Çiner, A., "Zara güneyi (Sivas havzası) karasal-sığ denizel Miyosen çökellerinin litostratigrafisi ve fasiyes özellikleri", *MTA Dergisi*, 125, (2002), 65-88.
- [8]. Tüysüz, O., "Erzincan çevresinin jeolojisi ve tektonik evrimi", 2nd National Earthquake Engineering Conference, Union of Chambers of Turkish Engineers and Architects Chambers of Civil Engineers, (1993), 271-280.
- [9]. Çiner, A., Koşun, E., "Hafik güneyindeki (Sivas Havzası) Oligo-Miyosen yaşlı çökellerin stratigrafisi ve sedimentolojisi" *TPJD Bült.*, 8 (1966a), 16-34.
- [10]. Kurtman, F., "Sivas-Hafik-Zara ve imranlı bölgesinin jeolojik ve tektonik yapısı" *MTA Derg.*, 80 (1973), 1-32.
- [11]. Tatar, Y., "Kuzey Anadolu Fay zonunun Erzincan-Refahiye arasındaki bölümü üzerinde tektonik incelemeler" *Yerbilimleri Derg.*, 4 (1978), 201-236.
- [12]. Poisson, A. M., Guezou, J. C., Öztürk, A., İnan, S., Temiz, H., Gürsoy, H., Kavak, K., Özden, S., "Tectonic setting and evolution of the Sivas Basin, Central Anatolia, Turkey", *Int. Geol. Rev.*, 38 (1996), 838-853.
- [13]. Koçyiğit, A., Özkan, S., Rojay, B., "Examples from the forearc basin remnants at the active margin of northern Neo-Tethys: development and emplacement ages of the Anatolian Nappes, Turkey", *Metu Journal of Pure And Applied Sciences*, 21 (1988), 183-210.
- [14]. Yılmaz, A., "Çarpışma sonrası bir çanak örneği: Sivas Havzası, Türkiye", *Türkiye 10. Petrol Kongresi ve Sergisi Bildirileri*, (1994), 21-33.
- [15]. Kavak, K.S., İnan, S., "Savcun ve Karacaören (Ulaş-Sivas) yörelerinde Sivas havzası güney kenarındaki tektonostratigrafik özellikleri", *Yerbilimleri*, 23 (2001), 113-127.
- [16]. Rojay, B., Karaca, A., "Post-Miocene deformation in the south of the Galatean Volcanic Province, NW of Central Anatolia (Turkey)", *Turkish Journal of Earth Sciences*, 17 (2008), 653-672.
- [17]. Akpınar, Z., Gürsoy, H., Tatar, O., Büyüksaraç, A., Koçbulut, F., Piper, J. D., "Geophysical analysis of fault geometry and volcanic activity in the Erzincan Basin, Central Turkey: complex evolution of a mature pull-apart basin" *Journal of Asian Earth Sciences*, 116 (2016), 97-114.
- [18]. Arpat, E., Şarolu, F., "Türkiye'deki bazı önemli genç tektonik olaylar", *Bullet. Geol. Cong.* 18 (1975), 91-101.
- [19]. Özgül, N. Ç., Turşucu, A., Özyardımcı, N., Şenol, M., Bingöl, İ., Uysal, Ş., "Munzur Dağlarının jeolojisi, MTA Derleme Rap., No. (1981), 6995.
- [20]. Barka, A. A., "Some neotectonic features of the Erzincan basin", *Earthq. Symp. Spec. Publ.*, (1984), 115-125.
- [21]. Gökçen, S. L., Kelling, G., "Oligocene deposits of the Zara-Hafik region (Sivas, Central Turkey); evolution from storm-influenced shelf to evaporitic basin", *Geol. Rundschau*, 74 (1985), 139-153.
- [22]. Yılmaz, A., "Yukarı Kelkit Çayı ile Munzur Dağları arasındaki temel jeoloji özellikleri ve yapısal evrimi" *Türkiye Jeol. Kur. Bült.*, 28 (1985), 79-92.
- [23]. Barka, A. A., Gülen, L., "New constraints on the age and total offset of the North Anatolian Fault Zone: implications for tectonics of the Eastern Mediterranean Region", *METU Journal of Pure Applied Science*, 21 (1989), 39-63.
- [24]. Norman, T. N., "On the structural evolution of the melange belt, north of Hafik (Sivas), Central Turkey", *Türkiye 8. Petrol Kongresi Bildiriler kitabı*, Ankara, (1990).
- [25]. Koçyiğit, A., "Neotectonic structures and related landforms expressing the contractional and extensional strains along the North Anatolian Fault at the northwestern margin of the Erzincan basin, NE Turkey" *Bull. Tech. Univ.*, 44 (1991), 455-473.
- [26]. Aktimur, H. T., Sarıaslan, M., Keçer, M., Turşucu, A., Örcen, S., Yurdakul, M. E., Mutlu, G., Aktimur, S., 1988., Yıldırım, T., "Erzincan dolayının jeolojisi" *MTA Rapor No.* (1995), 9772.
- [27]. Emre, Ö., Duman T. Y., Kondo, H., Olgun, Ş., Özalp, S., Elmacı, H., "1/250 000 ölçekli Türkiye diri fay haritası serisi, Erzincan (NJ 37-3) Paftası", *MTA Rapor No.* (2012), 44.
- [28]. Atalay, Z., "Sivas'ın batı ve güneybatısındaki çökellerin stratigrafisi ve çökel ortamları, Sivas Baseni Oturumu", *Cumhuriyet Univ. Müh. Fak.*, (1993), 6-8.
- [29]. Bayhan, H., Baysal, O., "Güneş-Soğucak (Divriği-Sivas) yöresinin petrografik ve petrolojik incelenmesi", *TJK Bülteni*, 25 (1982), 1-13.
- [30]. Tunç, M., Özçelik, O., Tutkun, Z., Gökçe, A., "Divriği-Yakuplu-İliç-Hamo (Sivas) yöresinin temel jeoloji özellikleri", *Tr. J. Eng. And Envi. Scie.*, 15 (1993), 225-245.
- [31]. Yılmaz, A., Sümengen, M., Terlemez, İ., Bilgiç, T., "1/100000 ölçekli Türkiye jeoloji haritaları serisi. Sivas-G23 paftası", *MTA*, (1989), Ankara.
- [32]. Aktimur, H. T., Ateş, Ş., Atalay, Z., Tekirli, M. E., Yurdakul, M. E., "Munzur Dağları ile Çavuşdağı

- arasının jeolojisi” MTA Derleme Rapor No. (1988), 8320.
- [33]. Kurtman, F., “Munzurlarda Kemah ve Ovacık bölgelerine ait petrol istikşaf etüdü” MTA Petrol Şubesi Rap. No. (1961), 22.
- [34]. Özdemir, C., İçen, C., “Erzincan İli İliç İlçesi ve civarı demir etütleri raporu”, MTA Rapor No. (1971), 4461.
- [35]. Aktimur, H. T., Tekirli, M. E., Yurdakul, M. E., “Sivas-Erzincan Tersiyer Havzasının jeolojisi” MTA Derg., 111, (1990), 25-36.
- [36]. Temiz, H., “The role of thrust ramp reactivation in pull-apart mechanism of the Erzincan basin, North Anatolian Fault Zone, Turkey”, *Geodinam. Acta*, 17, (2004), 219–228.
- [37]. Schreiber, B. C., Freidman, G. M., Decima, A., Schreiber, E., “Depositional environments of Upper Miocene (Messinian) evaporite deposits of the Silician Basin”, *Sedimentology*, 23, (1976), 729–760.
- [38]. Shearman, D. J., “Origin of marine evaporites by diagenesis” *Trans. Inst. Min. Metal.*, 75 (1966), 208-215.
- [39]. Warren, J. K., Kendall, G. C. S. C., “Comparison of marine sabkhas (subareial) and saline (subaqueous) evaporites: Modern and ancient”, *Bull. Am. Assoc. Petrol. Geol.*, 69, (1985), 1013-1023.
- [40]. Warren, J. K., “Evaporites: sediments, resources and hydrocarbons”, (2006) Springer, Berlin.
- [41]. Garrison, R. E., Schreiber, B. C., Bernoulli, D., Fabricius, F. H., Kidd, R. B., Melieres, F., “Sedimentary petrology and structures of Messinian evaporitic sediments in the Mediterranean Sea,” *Ini. Rep. Deep Sea Drill. Pro.*, 42, (1978), 571-611.
- [42]. Babel, M., “Models for evaporite, selenite and gypsum microbialite deposition in ancient saline basins”, *Acta Geologica Polonica*, 54, (2004), 219–249.
- [43]. Schreiber, B. C., Babel, M., Lugli, S., “Evaporites through Space and Time”, *Geological Society, London Special Publications*, 285, (2007), 1-13.
- [44]. Cody, R. D., “Lenticular gypsum: occurrences in nature, and experimental determinations of effects of soluble green plant material on its formation”, *J. Sed. Pet.*, 49, (1979), 1015–1028.
- [45]. Cody, R. D., Cody, A. M., “Gypsum nucleation and crystal morphology in analog saline terrestrial environments”, *J. Sediment. Petrol.*, 58 (1988), 247–255.
- [46]. Shearman, D. J., Orti, F., “Upper Miocene gypsum: San Miguel de Salinas, SE Spain”, *Soc. Geol. Ital.*, 16, (1976), 327–339.
- [47]. Warren, J. K., “The hydrological setting, occurrence and significance of gypsum in the late Quaternary salt lakes in South Australia”, *Sedimentology*, 29, (1982), 609–637.
- [48]. Manzi, V., Lugli, S., Ricci Lucchi, F., Roveri, M., “Deepwater clastic evaporites deposition in the Messinian Adriatic foredeep (northern Apennines, Italy): did the Mediterranean ever dry out?”, *Sedimentology*, 52, (2005), 875-902.
- [49]. Carrillo, E., Rosell, L., Ortí, F., “Multi-episodic evaporite sedimentation as an indicator of palaeogeographic evolution in foreland basins (Southeastern Pyrenean basin, Early–Middle Eocene)”, *Sedimentology*, 61, (2014), 7.
- [50]. Kinsman, D. J. J., “Models of formation, sedimentary associations and diagnostic features of shallow water and supratidal evaporites”, *Am. Assoc. Petr. Geol.*, 53, (1969), 830-840.
- [51]. Caldwell, R. H., “Holocene gypsum deposits of the Bullara Sunkland, Carnarvon Basin, Western Australia”, Thesis, Univ. Western Australia, (1976), 123.
- [52]. Hardie, L. A., Smooth, J. P., Eugster, H. P., “Saline lakes and their deposits”, *Sedimentology*, 2, (1978), 7-41.
- [53]. El-Tabakh, M., Riccioni, R., Schreiber, B. C., “Evolution of Late Triassic rift basin evaporites (Passaic Formation); Newark Basin, eastern North America”, *Sedimentology*, 44 (1997), 767–790.
- [54]. Arakel, A. V., “Genesis and diagenesis of Holocene evaporitic sediments in Hurt and Leeman Lagoons, western Australia”, *J. Sediment. Petrol.*, 50, (1980), 1305-1326.
- [55]. Magee, J. W., “Late Quaternary Lacustrine, groundwater, aeolian pedogenic gypsum in the Prungle lakes, Southeastern Australia”, *Paleogeography, Paleoclimatology-Paleoecology*, 84, (1991), 3–42.
- [56]. Ogniben, L., “Inverse graded bedding in primary gypsum of chemical deposition”, *J. Sed. Petrology*, 25, (1955), 273-281.
- [57]. Arzaghi, I. S., Khosrow-Tehrani, K., Afghah, M., “Sedimentology and petrography of Paleocene–Eocene evaporites: The Sachun Formation, Zagros Basin”, *Carbonates Evaporites*, 27, (2012), 43–53.
- [58]. Çiner, A., Koşun, E., Deynoux, M., “Fluvial, evaporitic and shallow-marine facies architecture, depositional evolution and cyclicity in the Sivas Basin (Lower to Middle Miocene, Central Turkey)”, *J. Asian Earth Sci.*, 21, (2002), 147-165.

- [59]. Aref, M. A., Basyoni, M. H., Bachmann, G. H., “Microbial and physical sedimentary structures in modern evaporitic coastal environments of Saudi Arabia and Egypt”, *Facies* 60, (2014), 371–388.
- [60]. Hardie, L. A., “Evaporites: Marine or non-marine” *Amer. Jour. Scien.*, 284, (1984), 193–240.
- [61]. Hardie, L. A., Lowenstein, T. K., Spencer, R. W., “The problem of distinguishing between primary and secondary features in evaporites”, *Salt Institute*, 1, (1985), 11–39.
- [62]. Reineck, H. E., Singh, I. B., “Depositional Sedimentary environments”, Springer verlag, Berlin, (1975), 549.
- [63]. Orti, F., Rosell, L., “Evaporite systems and diagenetic patterns in the Calatayud Basin (Miocene, central Spain)” *Sedimentology*, 47, (2000), 665–685.
- [64]. Peryt, T. M., Ortí, F., Rosell, L., “Sulfate platform-basin transition of the lower Werra Anhydrite (Zechstein, Upper Permian), western Poland: facies and petrography”, *Journal of Sedimentary Petrology*, 63, (1993), 646–658.
- [65]. Kendall, A. C., “Evaporites. Facies Models-response to sea level change”, *Geological Association of Canada, St John’s*, (1992), 375–409.
- [66]. Ortí, F., Salvany, J. M., “Coastal salina evaporites of the Triassic–Liassic boundary in the Iberian Peninsula: The Alacón borehole”, *Geologica Acta*, 2, (2004), 291–304.
- [67]. Orti, F., Salvany, M., “Continental evaporitic sedimentation in the Ebro Basin during the Miocene. Sedimentary Deposition in Rift and Foreland Basins in France and Spain (Paleogene and Lower Neogene)”, *Columbia University Press, New York*, (1997), 420–430.
- [68]. Holliday, D. W., “The petrology of secondary gypsum rocks”, *Journal of Sedimentary Petrology*, 40, (1970), 734–744.
- [69]. Abdioğlu, E., Arslan, M., Kadir, S., Temizel, İ., “Alteration mineralogy, lithochemistry and stable isotope geochemistry of the Murgul (Artvin, Ne Turkey) volcanic hosted massive sulfide deposit: implications to alteration age and ore forming fluids”, *Ore Geol. Rev.*, 66, (2015), 219–242.
- [70]. Orti, F., Rosell, L., “Sulfatos evaporíticos de interés petrologico (In Spanish)”, *Edicions Universitat de Barcelona, Fundacio Folch*, (1997).
- [71]. Forjanés, P., Astilleros, J. M., Fernández-Díaz, L., “The Formation of barite and celestite through the replacement of gypsum”, *Minerals*, 10, (2020), 189.
- [72]. Kushnir, J., “The composition and origin of brines during the Messinian desiccation event in the Mediterranean basin as deduced from concentrations of ions coprecipitated with gypsum and anhydrite” *Chern. Geol.*, 35, (1982), 333–350.
- [73]. Lan, X. H., “Clay minerals as an index of paleoclimate. Geological Science and Technology Information”, 9, (1990), 31 – 35.
- [74]. Kovacs, G. T., Morgan, G., Levine, M., McCrann, J., “The Australian community overwhelmingly approves IVF to treat subfertility, with increasing support over three decades”, *Obstetr Gynaecol*, 52, (2012), 302– 304.
- [75]. Temel, A., Gençoğlu, H., Bayhan, H., Öner, F., Ağrı, H., “Meke Dere (Güzelyurt-Aksaray) kaolinit ocağının hidrotermal mineral oluşumları”, *VII. Ulusal Kil Sempozyumu*, (1995), 76–87.
- [76]. Scholle, P. A., Ulmer, D. S., Melim, L. A., “Late-stage calcites in the Permian Capitan Formation and its equivalents, Delaware Basin margin, west Texas and New Mexico: evidence for replacement of precursor evaporites”, *Sedimentology*, 39, (1992), 207–234.
- [77]. Pryor, W. A., “Biogenic sedimentation and alteration of argillaceous sediments in shallow marine environments”, *Geological Society of America Bulletin*, 86, (1975), 1244–1254.
- [78]. Deik, H., Reuning, L., Petrick, B., Takayanagi, H., “Hardened faecal pellets as a significant component in deep water, subtropical marine environments”, *A Jour. Inter. Assoc. Sedim.*, (2019), DOI: 10.1002/dep2.64
- [79]. Tucker, R. M., “Giant polygons in the Triassic salt of Cheshire, England: a thermal contraction model for their origin”, *J. Sediment. Pet.*, 51, (1981), 779–786.
- [80]. Playa, E., Orti, F., Rosell, L., “Marine to non-marine sedimentation in the upper Miocene evaporites of the Eastern Betics, SE Spain: sedimentological and geochemical evidences”. *Sed. Geol.*, 133, (2000), 135–166.
- [81]. Hardie, L. A., Eugster, H. P., “The depositional environment of marine evaporites: a case for shallow, clastic accumulation” *Sedimentology*, 16, (1971), 187–220.